Chemical Science

ROYAL SOCIETY OF CHEMISTRY

EDGE ARTICLE

View Article Online
View Journal | View Issue

Cite this: *Chem. Sci.*, 2020, **11**, 5028

All publication charges for this article have been paid for by the Royal Society of Chemistry

Dynamic reaction-induced phase separation in tunable, adaptive covalent networks†

Katie M. Herbert, ‡[a] Patrick T. Getty,‡[a] Neil D. Dolinski, [a] Jerald E. Hertzog,[b] Derek de Jong,[c] James H. Lettow, [a] Joy Romulus,[d] Jonathan W. Onorato, [d] Elizabeth M. Foster[d] and Stuart J. Rowan *[abe]

Received 31st January 2020
Accepted 25th April 2020

DOI: 10.1039/d0sc00605j

rsc.li/chemical-science

A series of catalyst-free, room temperature dynamic bonds derived from a reversible thia-Michael reaction are utilized to access mechanically robust dynamic covalent network films. The equilibrium of the thiol addition to benzalcyanoacetate-based Michael-acceptors can be directly tuned by controlling the electron-donating/withdrawing nature of the Michael-acceptor. By modulating the composition of different Michael-acceptors in a dynamic covalent network, a wide range of mechanical properties and thermal responses can be realized. Additionally, the reported systems phase-separate in a process, coined dynamic reaction-induced phase separation (DRIPS), that yields reconfigurable phase morphologies and reprogrammable shape-memory behaviour as highlighted by the heat-induced folding of a predetermined structure.

Introduction

Dynamic covalent networks (DCNs), also known as covalent adaptable networks (CANs), are polymeric networks that incorporate dynamic covalent chemistries (DCCs) which enable the formation of functional, responsive systems.[1–7] Under ideal conditions, these dynamic covalent bonds undergo bond exchange without the encumbrance of unwanted side reactions.[8,9] The incorporation of a range of dynamic chemistries such as transesterification,[10–12] Diels–Alder reactions,[13–16] disulfide bonds,[17–19] and boronic esters[20–22] into materials has given researchers access to adaptive materials that exhibit self-healing, reprocessibility, stress relaxation, adhesion, and shape-memory properties.[23,24] The thia-Michael (tM) reaction, typically described as the base- or nucleophile-catalyzed addition of a thiol across an α,β-unsaturated carbonyl compound, has been a staple synthetic technique in polymer chemistry and materials science for decades.[25] While its reputation as a versatile reaction is well established, its ability to act as a reversible bond has only recently begun to be investigated in the realm dynamic polymer networks.[5,26–31]

In 2016, Konkolewicz and coworkers demonstrated that thiol-acrylate-based polymer networks are thermally-reversible at elevated temperatures (90 °C), affording such properties as healing and malleability.[26] The same group also reported pH-responsive tM systems in which thiol-maleimide adducts were shown to be reversible under basic conditions, again leading to healable films.[27] Using an alternative approach, Ishibashi and Kalow employed a Meldrum's acid derivative capable of reversibly crosslinking siloxane polymers containing pendant thiol groups without the use of a catalyst.[28] They showed that the resulting silicone network could be reprocessed *via* compression molding (150 °C, 9 tons, 15 minutes) at least ten times without significant loss of mechanical properties, demonstrating the viability of a catalyst-free approach to dynamic tM polymer networks. While these approaches elegantly demonstrate the utility of tM adducts as reversible bonds for responsive, reprocessable materials, they rely on basic conditions and/or high operating temperatures to access the desired dynamic behaviour, potentially limiting the application scope.

An interesting subset of the tM reaction with the potential to expand the capabilities of previously reported systems is the thiol addition to benzalcyanoacetate Michael-acceptors, Fig. 1. Pioneering small molecule studies by Taunton,[32] Anslyn,[33] and Houk[34] have shown that thiol addition to such Michael acceptors requires no catalyst and is dynamic at room temperature. The latter fact caught our attention as one class of dynamic covalent networks that has received little attention are those in which the bonds are dynamic at room

[a]*Pritzker School of Molecular Engineering, University of Chicago, Chicago, IL 60637, USA. E-mail: stuartrowan@uchicago.edu*

[b]*Department of Chemistry, University of Chicago, Chicago, IL 60637, USA*

[c]*The University of Chicago Laboratory Schools, 1362 E. 59th St., Chicago, IL 60637, USA*

[d]*Department of Macromolecular Science and Engineering, Case Western Reserve University, 2100 Adelbert Road, Cleveland, OH 44106, USA*

[e]*Chemical Science and Engineering Division and Center for Molecular Engineering, Argonne National Laboratory, 9700 S. Cass Ave., Lemont, IL 60434, USA*

† Electronic supplementary information (ESI) available: Supplementary results and video. See DOI: 10.1039/d0sc00605j

‡ These authors contributed equally.

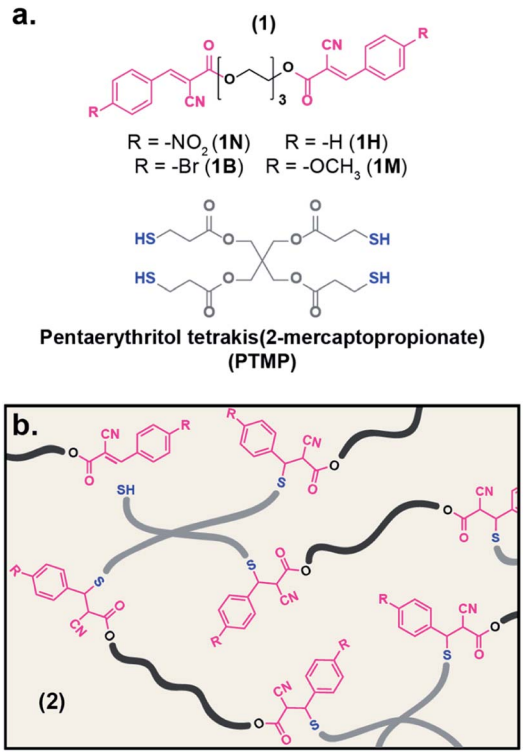

Fig. 1 (a) Chemical structures of ditopic electrophiles (1) and tetrathiol crosslinker, PTMP. (b) Illustration depicting the network formation of electrophiles associated/dissociated with PTMP (2).

temperature.[13,35] In addition, it has been shown that the presence of electron-donating or electron-withdrawing species on the β-phenyl ring alters the kinetics and thermodynamics of the reaction without drastically modifying the reactive site.[33] The ability to tune the strength of interactions has been well established as a means to control materials properties in non-covalent systems such as Lewis pairs[36] and metal–ligand interactions.[37,38] As such, these modular benzalcyanoacetates are a promising moiety for the preparation of tailorable materials. Despite these favourable properties, there have been very limited studies using this class of dynamic covalent bond in polymeric systems. The amide-based derivative, benzalcyanoacetamide, has been explored by Schubert, Hager and co-workers in organic solvent and in bulk polymeric systems. However, the reported benzalcyanoacetamide networks utilized basic conditions (specifically using 1,8-diazabicyclo(5.4.0)undec-7-ene, DBU) which ultimately led to the irreversible decomposition of the thiol component into H_2S gas.[29] It was later discovered that the same benzalcyanoacetamide motif could be used without degradation by eliminating the DBU in a bulk polymer system.[30] The acetate-based acceptors, on the other hand, have been largely set aside presumably due to their reported instability in the presence of water.[33] Preliminary results by Anslyn showed that the benzalcyanoacetate acceptors are indeed capable of participating in thiol-Michael addition although the aqueous conditions applied in those experiments resulted in hydrolysis of the benzalcyanoacetate through a retro-Knoevenagel reaction.[33]

Bonds that undergo active exchange at room temperature represent an attractive avenue for tuning materials properties at ambient conditions. However, without some form of reinforcement, these systems would likely flow freely and lack robust mechanical properties. One potential avenue of reinforcement, widely utilized in polymeric systems, is reaction/polymerization induced phase separation (RIPS/PIPS), whereby the evolution of the polymeric structure creates regions of dissimilar viscoelastic properties (*i.e.* viscosity, crosslink density, insolubility) that constitute the various phases throughout the films.[39–42] It is important to note that there have been recent reports of phase separated DCNs,[43–48] in which the materials primarily rely on dissimilar polymeric blocks to induce phase separation and an enhancement in mechanical properties is observed with such systems.

With the goal of harnessing the tunable, catalyst-free, room temperature, dynamic nature of the benzalcyanoacetate-based tM reaction in polymeric systems, this report first explores the dynamic bonding of the thiol addition to small molecule benzalcyanoacetate controls in organic media. Inspired by the apparent tunability of the tM reaction in solution, the investigation expands into bulk polymeric films based on the benzalcyanoacetate motif. These dynamic tM films show a wide range of mechanical properties, which is related to both the nature of the dynamic bond and the fact that these films exhibit phase separated morphologies, in a process termed here dynamic reaction-induced phase separation (DRIPS). The results demonstrate the ability of this tM reaction to tailor materials properties in adaptable networks, highlighting their DRIPS morphologies and shape memory behaviour.

Results and discussion

To probe a range of these tM dynamic bonds, a series of four benzalcyanoacetate compounds were synthesized (Fig. 2a). Each compound was differentiated by the electron-withdrawing/-donating capabilities of the substituent on the *para*-position of the β-phenyl ring (**mono-X**), namely nitro- (**mono-N**), bromo- (**mono-B**), hydrogen- (**mono-H**), and methoxy-substituted (**mono-M**).

The benzalcyanoacetate species were synthesized *via* a Knoevenagel condensation of methyl cyanoacetate with the corresponding benzaldehyde. To compare these Michael-acceptors to previous examples, the benzalcyanoacetate species were titrated with 1-octanethiol in anhydrous deuterated dimethyl sulfoxide (d_6-DMSO) at room temperature following NMR titration procedures and considerations outlined by Thordarson.[49] The titration experiments determined the equilibrium constant (K_{eq}) of the **mono-X** acceptors in d_6-DMSO to be *ca.* 470, 160, 60, and 10 M^{-1}, respectively (Fig. S2 and 3, Table S2†). Consistent with Anslyn's previous work, a Hammett plot of the equilibrium constants (Fig. 2b) reveals a positive trend, with $\rho = 1.46$ suggesting a system whose equilibrium properties are dictated by the electronic nature of the β-phenyl substituent.[33] As an interesting note, the apparent downward curvature of the data shown in the Hammett plot was also observed by Anslyn and suggests there may be variability in

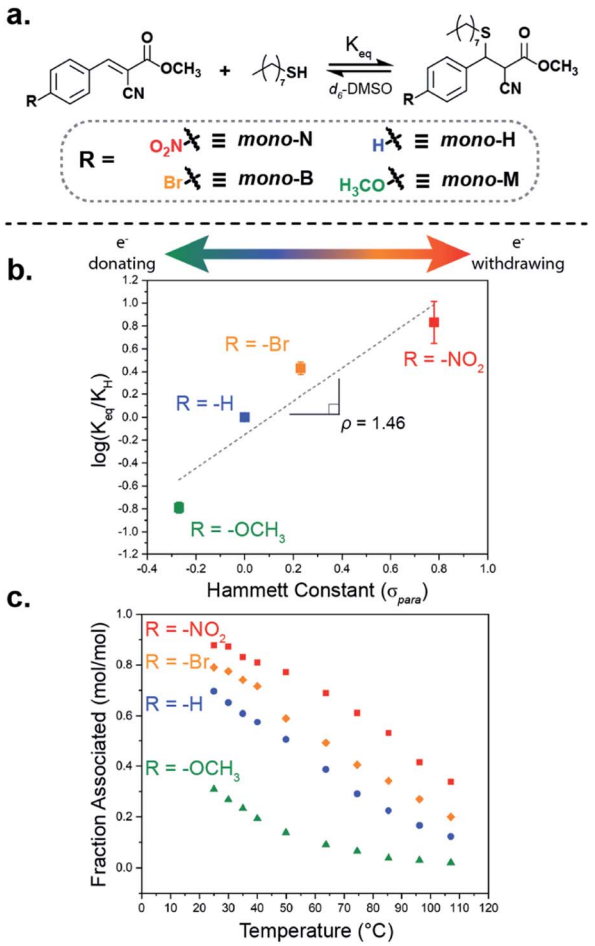

Fig. 2 (a) Schematic of benzalcyanoacetate electrophile equilibrium reaction with 1-octanethiol, (b) Hammett plot of equilibrium constants at room temperature in d_6-DMSO, and (c) equilibrium position of association as a function of temperature for **mono-N** (red), **mono-B** (orange), **mono-H** (blue), and **mono-M** (green) derivatives at 100 mM concentrations in d_6-DMSO.

the overall mechanism of dynamic exchange depending on the electronic nature of the Michael acceptor.

To further investigate the impact of the electronic substituent on bond formation, the equilibrium position of equimolar (100 mM) mixtures of thiol and **mono-X** was measured as a function of temperature in d_6-DMSO from ambient temperatures to *ca.* 110 °C (Fig. 2c). As expected, the fraction of the associated tM adduct observed decreased with increasing temperature, while maintaining the overall equilibrium trend (**mono-N** > **mono-B** > **mono-H** > **mono-M**) throughout the temperature range. Additionally, evaluation of these equilibrium values in a van't Hoff plot shows that the differences in bonding are primarily enthalpic (Fig. S5 and Table S3†). The thermal response of the thia-Michael equilibrium in these small molecule models anticipates two key properties in networks composed of these species: (1) a thermoresponsive material whose mechanical properties adapt to temperature and (2) a variation in total adduct formation at room temperature corresponding to a tunable effective crosslink density. As such, utilization of these electronically different Michael-acceptors in dynamic networks, should allow for direct control over the effective crosslinking of the networks, enabling the precise tuning of their properties.

To expand the small molecule studies to network systems, a series of ditopic acceptor compounds (**1**, Fig. 1a) were prepared with nitro- (**1N**), bromo- (**1B**), hydrogen- (**1H**), and methoxy-substituted (**1M**) benzalcyanoacetate moieties on the chain ends of a triethylene glycol core.[50] A tetrathiol crosslinker, pentaerythritol tetrakis(2-mercaptopropionate) (PTMP), and **1** were mixed in chloroform and cast onto a Teflon® dish to yield a film of the resultant tM network (**2**, Fig. 1b) after drying. The dried films were then compression molded at elevated temperature (10 kPSI, 70–90 °C), resulting in robust polymeric films approximately 400 μm thick. For consistency amongst the prepared networks, the ratio of reactive sites (thiol : alkene) was kept constant to a 1 : 1 ratio. The resulting samples are denoted $\mathbf{2N}_x$, $\mathbf{2B}_x$, $\mathbf{2H}_x$, and $\mathbf{2M}_x$ to indicate the use of **1N**, **1B**, **1H**, and **1M**, respectively, to form the network. The x relates the mole percent (mol%) of each acceptor site ($x = 100$ or 50 for hybrid networks) relative to the thiol groups.

The tM networks were studied *via* Raman spectroscopy to assess the degree of formation of the thia-Michael linkages within the bulk network, specifically focusing on the nitrile regime (C≡N stretch, 2260–2200 cm^{-1}). The spectra of the neat acceptors (**1N**, **1B**, **1H**, and **1M**) reveal a single peak at *ca.* 2226 cm^{-1} resulting from the stretching vibration of the conjugated C≡N bond. Once a thiol adds to the acceptor across the double bond, conjugation is lost and the C≡N signal shifts to higher frequencies, allowing for direct monitoring of adduct formation in the solid state (Fig. 3). In agreement with the model small molecule studies, the amount of adduct formed within the networks is highly dependent on the electronic nature of the β-phenyl substituent, with the more electron-withdrawing acceptors in $\mathbf{2N}_{100}$ reacting almost completely with the thiols (Fig. 3a, *ca.* 92% reacted by peak maximum), the electron-neutral groups in $\mathbf{2H}_{100}$ displaying a middling amount of adduct formation (Fig. 3c, *ca.* 85% reacted by peak maximum), while the electron-donating compounds in $\mathbf{2M}_{100}$ exhibit a significant amount of unreacted acceptor species (Fig. 3d, *ca.* 24% reacted by peak maximum). It is worthwhile noting however, that $\mathbf{2B}_{100}$ has an anomalously high relative concentration of unreacted species (Fig. 3b, only *ca.* 58% reacted by peak maximum) attributed to sample crystallinity as discussed below.

In addition to the shift in the C≡N stretch, there is a corresponding decrease in the thiol peak intensity at 2570 cm^{-1} as a result of the PTMP reactive groups participating in the crosslinking reaction (Fig. S6A†). As the reduction in the amount of free thiols could equally be attributed to disulfide formation within the network, the spectra were compared to a control sample crosslinked *via* disulfide bonds; however, no notable disulfide bond was observed in the tM films (Fig. S6B†).

Given that the extent of tM linkages should directly influence the mechanical properties of the networks, a series of experiments was conducted to elucidate the bulk properties of the tM systems. To measure the response of the tM films to uniaxial

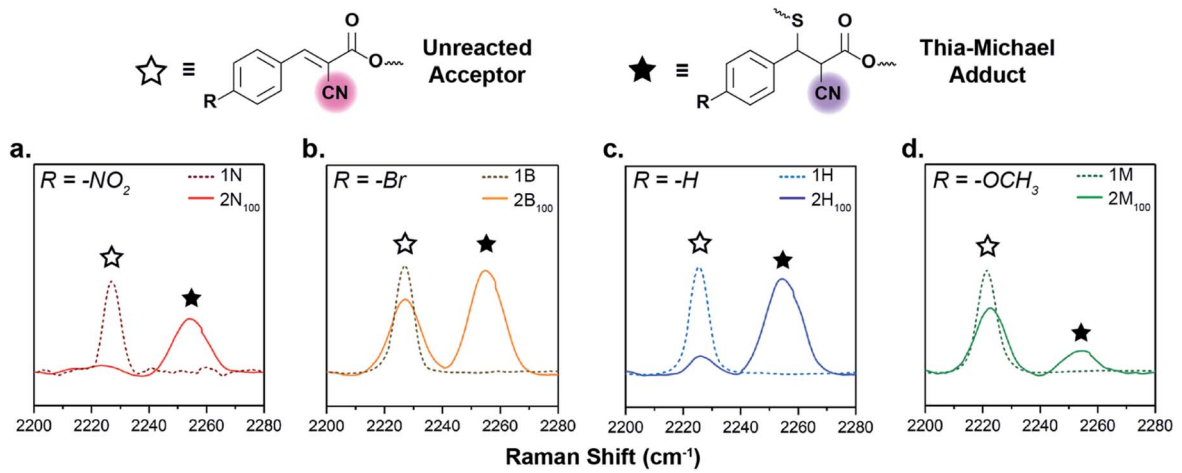

Fig. 3 Raman spectra of C≡N vibrational stretches for the neat electrophiles (dotted lines) overlaid with the respective thia-Michael networks (solid lines). (a) **1N** and $2N_{100}$, (b) **1B** and $2B_{100}$, (c) **1H** and $2H_{100}$, and (d) **1M** and $2M_{100}$.

tension, rectangular strips of $\mathbf{2N_{100}}$ and $\mathbf{2H_{100}}$ were cut from the pressed films and uniaxially deformed at a rate of 10 mm min^{-1} in ambient conditions. Unfortunately, neither $\mathbf{2B_{100}}$ nor $\mathbf{2M_{100}}$ formed films suitable for tensile testing (likely a result of film crystallinity/inadequate crosslinking) and were therefore excluded from further mechanical tests. As expected, films formed using different acceptors exhibited distinctive mechanical properties at room temperature (Fig. 4a), with $\mathbf{2N_{100}}$ displaying the highest stress at break (20 ± 3 MPa) and very little ductility (strain at break = 1.5 ± 0.3%). Conversely, $\mathbf{2H_{100}}$ exhibited a much lower ultimate strength (0.17 ± 0.03 MPa), but stretched to more than 700% of its original length. In an effort to better assess the impact of the different Michael acceptors on mechanical properties, a series of hybrid materials, $\mathbf{2N_{50}B_{50}}$, $\mathbf{2N_{50}H_{50}}$, $\mathbf{2N_{50}M_{50}}$, were also prepared, and resulted in robust films across the series. Interestingly, the hybrid material tensile properties were found to correlate strongly with the equilibrium binding studies, with $\mathbf{2N_{50}B_{50}} > \mathbf{2N_{50}H_{50}} > \mathbf{2N_{50}M_{50}}$ in terms of ultimate strength, and the opposite trend for overall sample ductility, which can be attributed in part to higher degrees of effective crosslinking with increasingly electron-withdrawing groups. It should be noted that this increase in crosslinking also increases the T_g of materials, leading to the stiff, relatively brittle character of $\mathbf{2N_{100}}$ and $\mathbf{2N_{50}B_{50}}$ at room temperature. To assess the impact of adding weaker bonds in the hybrid materials (particularly in the case of $\mathbf{2N_{50}M_{50}}$) control studies using $\mathbf{2N_{50}}$ samples were carried out. While $\mathbf{2N_{50}}$ and $\mathbf{2N_{50}M_{50}}$ samples displayed similar thermal properties (*i.e.* T_g), $\mathbf{2N_{50}}$ displayed significantly enhanced yield strength compared to the $\mathbf{2N_{50}M_{50}}$ film, suggesting that the weak-bonding **1M** species have a larger effect on the properties than simply diluting the concentration of the **1N** species (Fig S9†).

As temperature was shown to strongly influence the extent of adduct formation in the model studies, the effect of temperature on mechanical behaviour was evaluated. As the moduli of these materials span several orders of magnitude, a combination of methods, namely dynamic mechanical analysis (DMA) and shear rheology, was used to describe their thermo-mechanical properties. The results of the DMA measurements (Fig. 4b) revealed the glass transition temperature (T_g, as defined by loss modulus [E''] peak, Fig. S10†) as 47.5 °C and 8.9 °C, for $\mathbf{2N_{100}}$ and $\mathbf{2H_{100}}$, respectively, in accordance with the distinct mechanical properties of the two networks at room temperature. In the hybrid networks, the combination of crosslinks within the system enabled a systematic tuning of T_g with $\mathbf{2N_{50}B_{50}}$, $\mathbf{2N_{50}H_{50}}$, and $\mathbf{2N_{50}M_{50}}$ exhibiting T_g at 39, 29 and 21 °C, respectively. Following this glass transition, a significant difference in performance within the plateau regime was also observed. Where $\mathbf{2N_{100}}$ exhibited a clear plateau on the order of 10^6 Pa, no plateau was observed in the $\mathbf{2H_{100}}$ film (under these experimental conditions). The hybrid materials followed the same trend observed in the tensile studies, with $\mathbf{2N_{50}B_{50}}$ and $\mathbf{2N_{50}H_{50}}$ behaving more similarly to $\mathbf{2N_{100}}$, yielding plateau behaviour above T_g while $\mathbf{2N_{50}M_{50}}$ did not exhibit a plateau.

To more accurately probe the performance of these materials at higher temperatures, shear rheology experiments were carried out. As can be seen in Fig. 4c, $\mathbf{2N_{100}}$ maintained a plateau up to *ca.* 125 °C whereas $\mathbf{2H_{100}}$ was weaker by two orders of magnitude and began its second transition at *ca.* 90 °C. The hybrid materials followed expected trends with $\mathbf{2N_{50}B_{50}}$ exhibiting a slightly higher plateau modulus and second transition temperature (*ca.* 180 kPa until *ca.* 122 °C) than $\mathbf{2N_{50}H_{50}}$ (*ca.* 110 kPa until *ca.* 117 °C). $\mathbf{2N_{50}M_{50}}$ lacked a stable plateau regime and demonstrated a second transition at *ca.* 101 °C. Thus, these initial evaluations demonstrate the ability to tailor both thermal and mechanical properties of dynamic networks through the use of dynamic bonds with different equilibrium behaviours.

Reflecting on the equilibrium adduct formation as a function of temperature, it is curious to note that certain samples exhibit a plateau (under these experimental conditions) at elevated temperatures. Flory–Stockmayer theory predicts that a system consisting of di- and tetrafunctional monomers, such as the $\mathbf{2N_{100}}$ network, would percolate above *ca.* 58% conversion

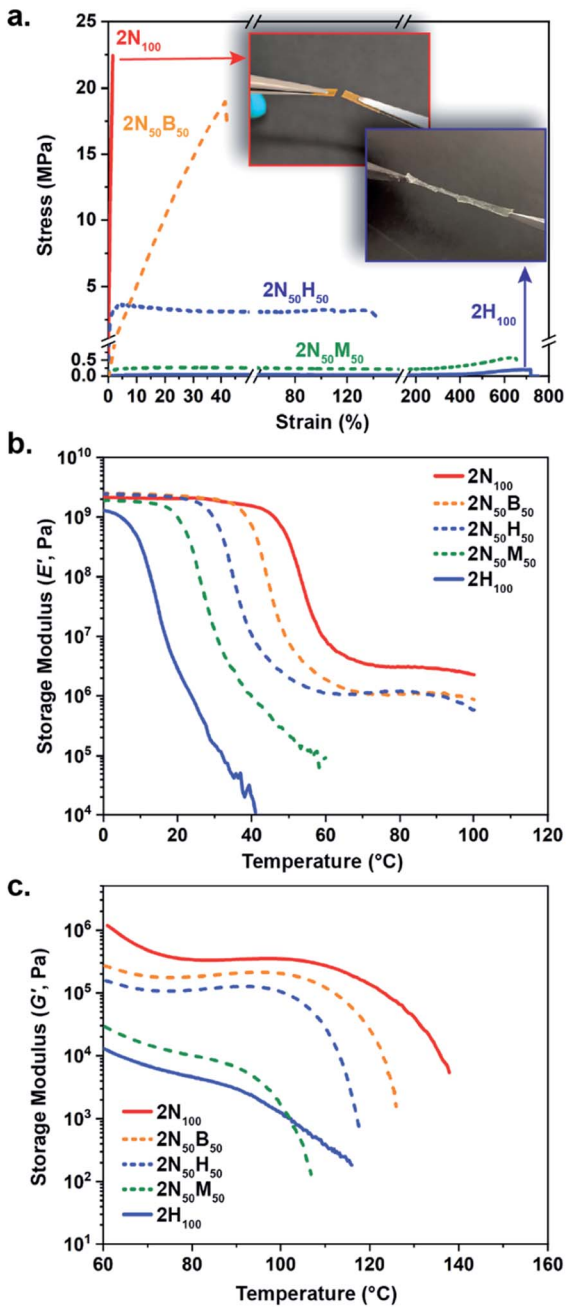

Fig. 4 (a) Stress–strain curves (strain rate = 10 mm min^{-1}, 25 °C), (b) dynamic mechanical analysis (DMA; temperature ramp rate = 3 °C min^{-1}, frequency = 1 Hz, tensile geometry) and (c) shear rheology (temperature ramp rate = 3 °C min^{-1}, frequency = 2 Hz, parallel plate geometry) curves for $2N_{100}$ (red), $2N_{50}B_{50}$ (dashed orange), $2N_{50}H_{50}$ (dashed blue), $2N_{50}M_{50}$ (dashed green), and $2H_{100}$ (blue).

(for a tetrafunctional monomer with a stoichiometric amount of a difunctional partner). Recalling the NMR temperature studies (Fig. 2c), this would imply that the $\mathbf{2N_{100}}$ film should lose connectivity at temperatures above ~75 °C assuming a homogeneous network construction. To investigate this seeming contradiction, differential scanning calorimetry (DSC) was carried out on all the films. Interestingly, the DSC traces confirmed the DMA experiments with all the networks exhibiting two distinct thermal transitions. While the trend in the lower transition temperatures (assigned as a T_g) is consistent with that observed in the DMA, there is also a broad second transition at much higher temperatures (>125 °C) (Fig. 5 and S11†), suggesting the presence of multiple phases in these dynamic films. The lone exception to dual transitions in the DSC is the $\mathbf{2B_{100}}$ film which exhibited multiple phase transitions at elevated temperatures, which are attributed to the cold-crystallization of the electrophile. This phase behaviour explains the previously discussed anomalies for the $\mathbf{2B_{100}}$ films, namely that crystallization of the electrophile results in the relatively high amount of unreacted Michael acceptor and the lack of robust film formation. Modulated DSC experiments on $\mathbf{2N_{100}}$ samples verify the lower temperature thermal transition has a high degree of reversing character, consistent with a T_g while the higher transition shows little to no reversing character, suggesting a more complex phase behaviour (Fig. S12†). The non-reversing character of the upper transition may potentially be explained by 'trapped' tM bonds in a densified hard phase possibly formed by highly reacted tM adduct oligomers crashing out of the solution or melt. As the matrix softens and the bonds are able to exchange, they rapidly dissociate in accordance with temperature dependent small molecule studies in Fig. 2c.

The dual phase transition behaviour was also observed in the DSC traces for the hybrid systems, with T_g values of these films tracking with equilibrium constant and higher values observed for networks formed from more thermodynamically stable dynamic bonds. Additionally, the onset of the lower temperature transition in the hybrid films reflects an approximate Fox-like blend of the glass transitions of the homo-Michael acceptor films (Fig. S13†). A similar trend was observed for the higher temperature transition, although the breadth of the transition in the hybrid films makes the precise transition temperature difficult to accurately compare.

As the thermal properties indicated a dual phase system, atomic force microscopy (AFM) of as-cast films (to avoid surface features transferred by compression molding) was undertaken

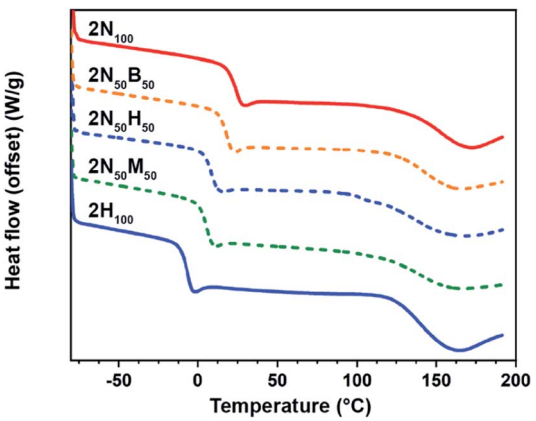

Fig. 5 Differential scanning calorimetry (DSC) curves for $2N_{100}$ (red), $2N_{50}B_{50}$ (dashed orange), $2N_{50}H_{50}$ (dashed blue), and $2N_{50}M_{50}$ (dashed green), $2H_{100}$ (blue).

to further elucidate the microphase morphology of the networks (Fig. 6). Although the high T_g of $\mathbf{2N_{100}}$ prevented differentiation of hard/soft regions, AFM phase images of both $\mathbf{2H_{100}}$ and $\mathbf{2M_{100}}$ clearly show dual-phase materials composed of a soft matrix (attributed to the lower thermal transition) with hard, circular inclusions (attributed to the higher thermal transition) (Fig. 6a and b). We hypothesize that while dynamic bonds exist in both phases, access to the dynamic exchange in either phase is restricted to the corresponding phase transition temperature. As such, in both cases, the connectivity of the overall film is primarily dictated by the dynamic behaviour of the soft phase, leading to the lack of a plateau above T_g for the $\mathbf{2H_{100}}$ and to weak films in the case of $\mathbf{2M_{100}}$. The hybrid films, on the other hand, revealed more complex morphologies, indicative of a combination of phase separation phenomena (Fig. 6c and d). For example, $\mathbf{2N_{50}H_{50}}$ reveals concentric phase development in which a continuous hard phase contains encapsulated softer phases, leading to a percolated network of the higher thermal transition phase, which explains the resulting plateau regime in the DMA above T_g. Similar phase behaviour was also observed in the case of $\mathbf{2N_{50}B_{50}}$ (Fig. S15†). In contrast, the $\mathbf{2N_{50}M_{50}}$ shows circular regions of two different phases (bright and dark phases in Fig. 6d inset and S16†) that are both distinct from the soft continuous phase, leading to a lack of plateau behaviour at elevated temperatures and the low yield strength in tension at room temperature.

As a result of the phase separated morphology and the presence of a plateau in the DMA, it was hypothesized that films formed *via* the dynamic reaction-induced phase separation (DRIPS) process should exhibit reprogrammable shape memory behaviour. In a representative example, the shape memory behaviour of the $\mathbf{2N_{50}H_{50}}$ film was evaluated using force-controlled DMA shape memory experiments. A single temporary shape was imparted to the sample at 60 °C and fixed upon cooling below T_g to room temperature, where the applied force was released (Fig. 7a). $\mathbf{2N_{50}H_{50}}$ demonstrated an ideal fixing ratio of 100%, showing no change in strain after the temporary shape was set (maximum strain, ε_m, and unloading strain, ε_u = 0.365). Upon reheating, the sample recovered to 90% of its original shape (recovery strain, ε_r = 0.0371), with the residual 10% likely lost on account of creep within the sample that occurred throughout the shape memory process (a phenomenon common to dynamic covalent materials). The ability to reprogram this behaviour was demonstrated by fixing a new permanent shape (Fig. 7b, Shape 1) in the film at elevated temperatures (90 °C), allowing the continuous stiff phase to relax and maintain Shape 1 upon cooling. Carrying out the

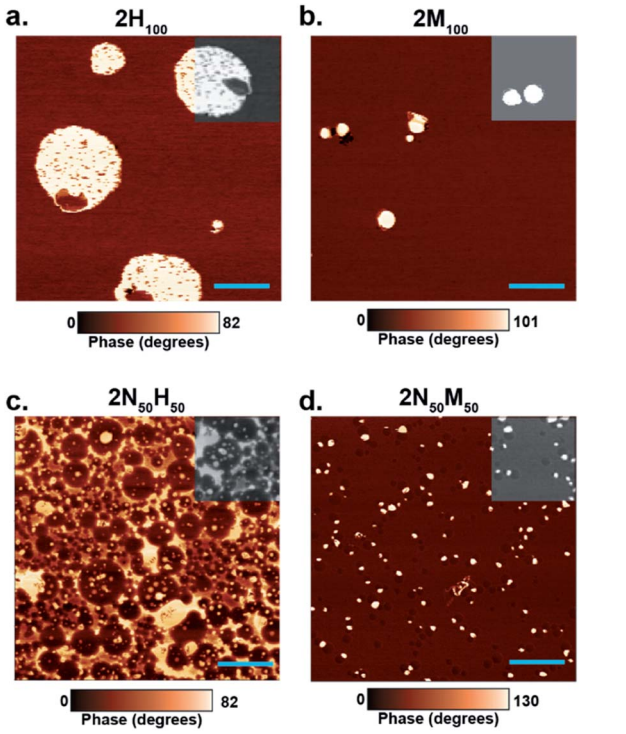

Fig. 6 Atomic force micrographs showing phase image, phase color scheme (bottom, dark = soft phase, light = hard phase). (a) $2H_{100}$, (b) $2M_{100}$, (c) $2N_{50}H_{50}$, (d) $2N_{50}M_{50}$ (top right corner of each image recolored to highlight shape outlines, not scaled to phase). Scale bar = 1 μm.

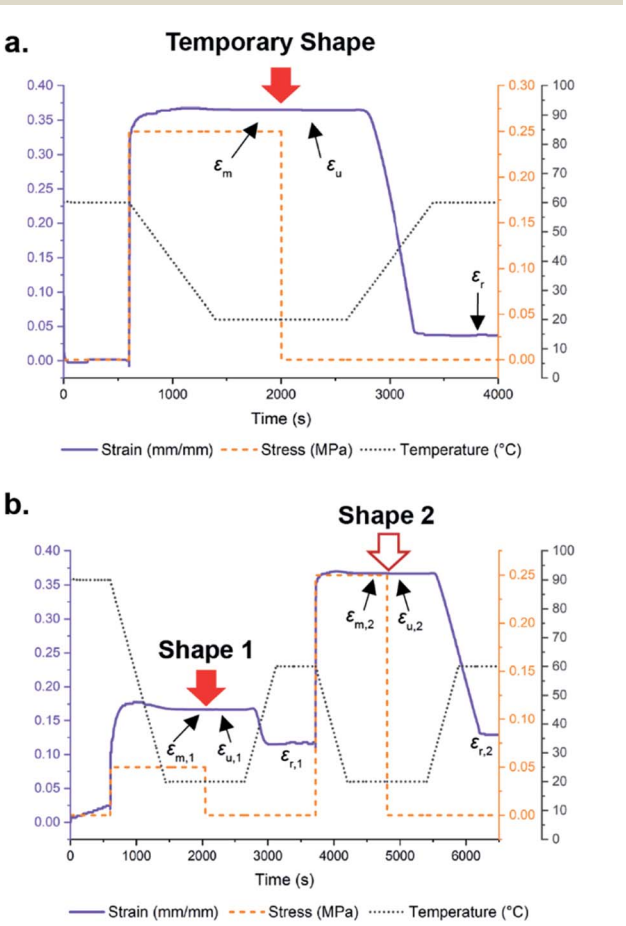

Fig. 7 Force-controlled dynamic mechanical analysis (DMA) experiments demonstrating (a) one-way and (b) reprogrammable shape memory behaviour of $2N_{50}H_{50}$. ε_m = maximum strain; ε_u = unloading strain; ε_r = recovery strain; sample size = *ca.* 10 mm × 4 mm × 0.5 mm (length × width × thickness).

previous conditions to impart a new temporary shape (Fig. 7b, Shape 2) into the material, once again demonstrated a 100% fixing ratio of Shape 2 followed by a 95% recovery back to the relaxed Shape 1 ($(\varepsilon_{m,2} - \varepsilon_{r,2}/\varepsilon_{m,2} - \varepsilon_{r,1}) \times 100$).

To further demonstrate the shape memory behaviour of these materials a sheet of $\mathbf{2N_{50}H_{50}}$ was prepared for a demonstration of self-folding. The capacity to trigger stimuli-responsive folding has attracted interest, for example, as a means to control soft robotics systems that can move, bend, and propel themselves through space.[51] Thus, by using the reprogrammable shape memory property of films formed *via* DRIPS, it was possible to program larger, complex architectures through simply folding (creasing) a flat film to a structure, such as the airplane in Fig. 8, that self-folds upon heating. This was accomplished by creasing a $\mathbf{2N_{50}H_{50}}$ film at elevated temperatures (over a hot plate at 105 °C) and subsequently cooling to room temperature, thereby programming the permanent shape into the folded geometry (Fig. 8a and S17†). The film was unfolded just above T_g (*ca.* 45 °C), cooled to room temperature, and fixed into a flat, temporary geometry that maintained the creases from folding, similar to those observed in a standard paper airplane (Fig. 8b). Upon heating again to >45 °C, the sample folded itself into a "plastic" airplane (Fig. 8c, see ESI for Video†).

Another potentially interesting property of dynamic reaction-induced phase separation (DRIPS) is the ability to thermally reprocess materials after casting to yield materials with new morphologies and properties *via* melt processing. This is distinct from standard RIPS/PIPS of network materials where the reaction/polymerization is irreversible. The incorporation of dynamic thia-Michael bonds into the network creates a fully reversible, tunable environment that allows the films to be reprocessed and reprogrammed. To demonstrate the impact of melt processing conditions on DRIPS, a solution cast sample of $\mathbf{2N_{50}H_{50}}$ was annealed at 200 °C (above the upper transition) for 30 minutes then either cooled slowly (1 °C min^{-1}) or quenched in liquid nitrogen (LN_2). This thermal treatment resulted in a drastically different phase structure and mechanical properties as compared to the non-annealed films (processed between thermal transitions) shown in Fig. 6. Annealing above the upper transition of $\mathbf{2N_{50}H_{50}}$ followed by slow cooling enables the formation of a much higher percentage of the hard phase which forms continuously throughout the material, resulting in a glassy, brittle film at room temperature (Fig. 9a and c) whereas quenching the material disrupted the continuity of the hard phase, yielding a soft, viscoelastic solid (Fig. 9b and d). This development of the phases was confirmed by DSC of a single sample cooled at various rates, demonstrating increased amounts of the high temperature phase with slower cooling rates (Fig. S18†). Additionally, the cooling rate directly impacts the lower thermal transition as well, with slower cooling rates (more hard phase) increasing the temperature of the lower

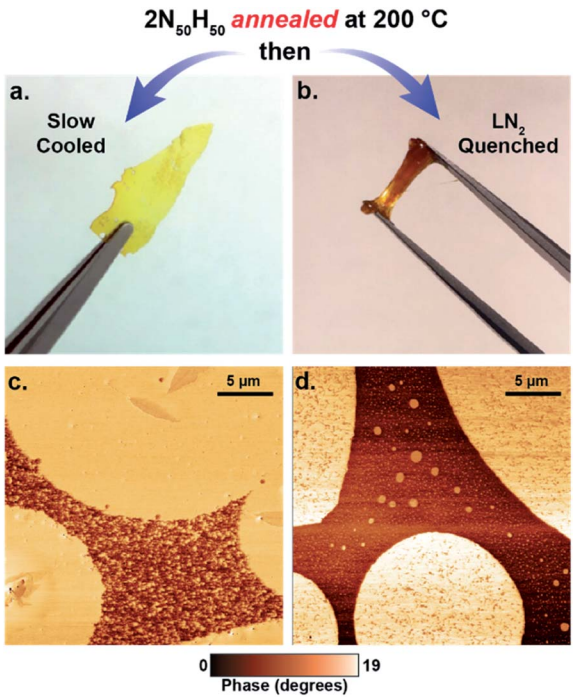

Fig. 9 Change in morphology of $\mathbf{2N_{50}H_{50}}$ after annealing at 200 °C then slow cooling (1 °C min^{-1}) to room temperature ((a) photograph and (c) AFM image) or quenching in liquid nitrogen ((b) photograph and (d) AFM image). Scale bar = 5 μm. Phase gradient applies to both (c) and (d).

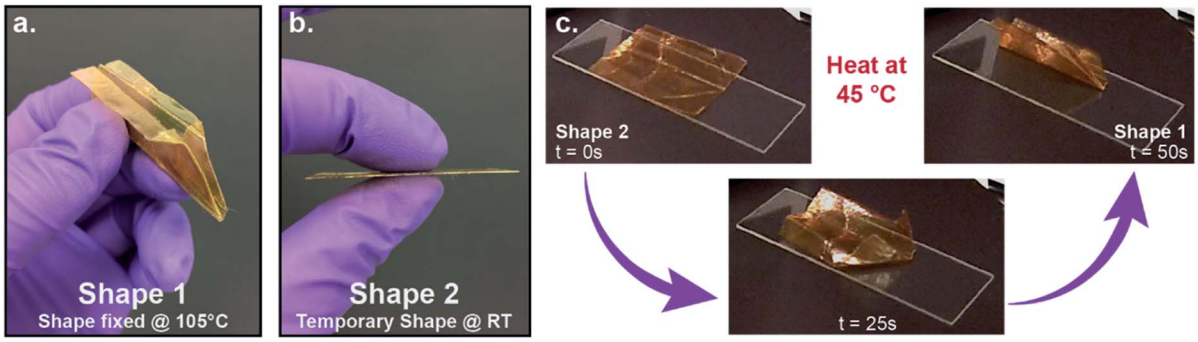

Fig. 8 Demonstration of reprogrammable shape memory behaviour of $\mathbf{2N_{50}H_{50}}$. (a) The programmed airplane shape fixed at 105 °C and cooled to room temperature, (b) same sample flattened into its temporary shape at room temperature, (c) time-lapse photos of the film folding into the programmed airplane shape upon exposure to heat.

transition, which is typical for glass transitions in, somewhat analogous, semi-crystalline polymer samples. These findings were further supported by shear rheology experiments in which a $\mathbf{2N_{100}}$ sample was thermally cycled at elevated temperatures (60–110 °C). Each cycle resulted in a steady increase in storage modulus, presumably a consequence of the growth of hard phase segments during heating and cooling cycles (Fig. S19†).

Conclusions

In summary, the combination of the tetrathiol PTMP with ditopic benzalcyanoacetate Michael acceptors grants access to dynamic networks with a wide range of thermomechanical properties. Furthermore, the electronic nature of the substituent on the acceptors has a direct effect on the equilibrium reaction of the thiols to the benzalcyanoacetate moieties. These differences in equilibrium can be used to directly manipulate the thermomechanical properties of these materials. Interestingly, even though these tM-adducts are dynamic at room temperature, it is possible to access mechanically robust films on account of a dynamic reaction-induced phase separation (DRIPS) process. In fact, the phase separation is critical to the properties of these materials and lends a complimentary handle for tuning the material properties. The phase-separated morphology of the films combined with their dynamic covalent chemistry gives rise to creaseable materials exhibiting reprogrammable shape memory. This behaviour was highlighted by the self-folding of a "paper/plastic airplane" structure along thermally-programmed folds. Ongoing research seeks to better understand the phase separation of these materials and to explore the potential of these easy-to-access, low temperature dynamic networks in a variety of applications including multi-stage low-temperature adhesives and self-folding actuators.

Conflicts of interest

There are no conflicts to declare.

Acknowledgements

This work was supported by the Division of Materials Research of the NSF (Award #1609076) and in part by NIST contract 60NANB15D077, the Center for Hierarchical Materials Design (CHiMaD). N.D.D. thanks the Pritzker School of Molecular Engineering for support through a postdoctoral fellowship. The authors thank Dr Phillip Griffin and Dr Justin Jureller for their helpful discussions. The authors also thank Arvin Sookezian for donating the disulfide network material used in the control Raman experiments. Parts of this work were carried out at the Soft Matter Characterization Facility and at the Materials Research Science and Engineering Center (MRSEC NSF DMR-1420709) at the University of Chicago.

References

1 C. J. Kloxin and C. N. Bowman, *Chem. Soc. Rev.*, 2013, **42**, 7161–7173.
2 C. N. Bowman and C. J. Kloxin, *Angew. Chem. Int. Ed.*, 2012, **51**, 4272–4274.
3 C. J. Kloxin, T. F. Scott, B. J. Adzima and C. N. Bowman, *Macromolecules*, 2010, **43**, 2643–2653.
4 R. J. Wojtecki, M. A. Meador and S. J. Rowan, *Nat. Mater.*, 2010, **10**, 14–27.
5 P. Chakma and D. Konkolewicz, *Angew. Chem. Int. Ed.*, 2019, **58**, 9682–9695.
6 S. Mukherjee, J. J. Cash and B. S. Sumerlin, *Dyn. Covalent Chem.*, 2017, 321–358.
7 G. M. Scheutz, J. J. Lessard, M. B. Sims and B. S. Sumerlin, *J. Am. Chem. Soc.*, 2019, **141**, 16181–16196.
8 S. J. Rowan, S. J. Cantrill, G. R. L. Cousins, J. K. M. Sanders and J. F. Stoddart, *Angew. Chem. Int. Ed.*, 2002, **41**, 898–952.
9 Y. Jin, C. Yu, R. J. Denman and W. Zhang, *Chem. Soc. Rev.*, 2013, **42**, 6634–6654.
10 D. Montarnal, M. Capelot, F. Tournilhac and L. Leibler, *Science*, 2011, **334**, 965–968.
11 H. Zhang, C. Cai, W. Liu, D. Li, J. Zhang, N. Zhao and J. Xu, *Sci. Rep.*, 2017, **7**, 11833.
12 J. L. Self, N. D. Dolinski, M. S. Zayas, J. Read de Alaniz and C. M. Bates, *ACS Macro Lett.*, 2018, **7**, 817–821.
13 P. Reutenauer, E. Buhler, P. J. Boul, S. J. Candau and J.-M. Lehn, *Chem.–Eur. J.*, 2009, **15**, 1893–1900.
14 P. M. Imbesi, C. Fidge, J. E. Raymond, S. I. Cauët and K. L. Wooley, *ACS Macro Lett.*, 2012, **1**, 473–477.
15 B. J. Adzima, H. Alan Aguirre, C. J. Kloxin, T. F. Scott and C. N. Bowman, *Macromolecules*, 2008, **41**, 9112–9117.
16 K. K. Oehlenschlaeger, J. O. Mueller, J. Brandt, S. Hilf, A. Lederer, M. Wilhelm, R. Graf, M. L. Coote, F. G. Schmidt and C. Barner-Kowollik, *Adv. Mater.*, 2014, **26**, 3561–3566.
17 B. T. Michal, E. J. Spencer and S. J. Rowan, *ACS Appl. Mater. Interfaces*, 2016, **8**, 11041–11049.
18 B. T. Michal, C. A. Jaye, E. J. Spencer and S. J. Rowan, *ACS Macro Lett.*, 2013, **2**, 694–699.
19 J. Canadell, H. Goossens and B. Klumperman, *Macromolecules*, 2011, **44**, 2536–2541.
20 J. J. Cash, T. Kubo, A. P. Bapat and B. S. Sumerlin, *Macromolecules*, 2015, **48**, 2098–2106.
21 A. P. Bapat, D. Roy, J. G. Ray, D. A. Savin and B. S. Sumerlin, *J. Am. Chem. Soc.*, 2011, **133**, 19832–19838.
22 O. R. Cromwell, J. Chung and Z. Guan, *J. Am. Chem. Soc.*, 2015, **137**, 6492–6495.
23 Z. P. Zhang, M. Z. Rong and M. Q. Zhang, *Prog. Polym. Sci.*, 2018, **80**, 39–93.
24 Q. Zhao, H. J. Qi and T. Xie, *Prog. Polym. Sci.*, 2015, **49–50**, 79–120.
25 D. P. Nair, M. Podgórski, S. Chatani, T. Gong, W. Xi, C. R. Fenoli and C. N. Bowman, *Chem. Mater.*, 2013, **26**, 724–744.
26 B. Zhang, Z. A. Digby, J. A. Flum, P. Chakma, J. M. Saul, J. L. Sparks and D. Konkolewicz, *Macromolecules*, 2016, **49**, 6871–6878.
27 P. Chakma, L. H. Rodrigues Possarle, Z. A. Digby, B. Zhang, J. L. Sparks and D. Konkolewicz, *Polym. Chem.*, 2017, **8**, 6534–6543.

28 J. S. A. Ishibashi and J. A. Kalow, *ACS Macro Lett.*, 2018, **7**, 482–486.
29 N. Kuhl, R. Geitner, R. K. Bose, S. Bode, B. Dietzek, M. Schmitt, J. Popp, S. J. Garcia, S. van der Zwaag, U. S. Schubert and M. D. Hager, *Macromol. Chem. Phys.*, 2016, **217**, 2541–2550.
30 N. Kuhl, R. Geitner, J. Vitz, S. Bode, M. Schmitt, J. Popp, U. S. Schubert and M. D. Hager, *J. Appl. Polym. Sci.*, 2017, **134**, 44805.
31 N. Van Herck, D. Maes, K. Unal, M. Guerre, J. M. Winne and F. E. Du Prez, *Angew. Chem. Int. Ed.*, 2020, **59**, 3609–3617.
32 I. M. Serafimova, M. A. Pufall, S. Krishnan, K. Duda, M. S. Cohen, R. L. Maglathlin, J. M. McFarland, R. M. Miller, M. Frödin and J. Taunton, *Nat. Chem. Biol.*, 2012, **8**, 471.
33 Y. Zhong, Y. Xu and E. V. Anslyn, *Eur. J. Org Chem.*, 2013, **2013**, 5017–5021.
34 E. H. Krenske, R. C. Petter and K. N. Houk, *J. Org. Chem.*, 2016, **81**, 11726–11733.
35 A. Rekondo, R. Martin, A. Ruiz De Luzuriaga, G. Cabañero, H. J. Grande and I. Odriozola, *Mater. Horiz.*, 2014, **1**, 237–240.
36 F. Vidal, J. Gomezcoello, R. A. Lalancette and F. Jäkle, *J. Am. Chem. Soc.*, 2019, **141**, 15963–15971.
37 M. S. Menyo, C. J. Hawker and J. H. Waite, *Soft Matter*, 2013, **9**, 10314–10323.
38 S. C. Grindy, R. Learsch, D. Mozhdehi, J. Cheng, D. G. Barrett, Z. Guan, P. B. Messersmith and N. Holten-Andersen, *Nat. Mater.*, 2015, **14**, 1210–1216.
39 R. J. J. Williams, B. A. Rozenberg and J.-P. Pascault, in *Polymer Analysis Polymer Physics. Advances in Polymer Science*, Springer, Berlin, Heidelberg, 1997, vol. 128, pp. 95–156.
40 K. Yamanaka, Y. Takagi and T. Inoue, *Polymer*, 1989, **30**, 1839–1844.
41 A. H. Torbati, H. B. Nejad, M. Ponce, J. P. Sutton and P. T. Mather, *Soft Matter*, 2014, **10**, 3112–3121.
42 Y. Liu, *J. Appl. Polym. Sci.*, 2013, **127**, 3279–3292.
43 L. Zhang, L. Chen and S. J. Rowan, *Macromol. Chem. Phys.*, 2017, **218**, 1600320.
44 M. Guerre, C. Taplan, R. Nicolaÿ, J. M. Winne and F. E. Du Prez, *J. Am. Chem. Soc.*, 2018, **140**, 13272–13284.
45 J. J. Lessard, G. M. Scheutz, S. H. Sung, K. A. Lantz, T. H. Epps and B. S. Sumerlin, *J. Am. Chem. Soc.*, 2020, **142**, 283–289.
46 X. Chen, L. Li, T. Wei and J. M. Torkelson, *Macromol. Chem. Phys.*, 2019, **220**, 1900083.
47 X. Chen, L. Li and J. M. Torkelson, *Polymer*, 2019, **178**, 121604.
48 R. G. Ricarte, F. Tournilhac and L. Leibler, *Macromolecules*, 2019, **52**, 432–443.
49 P. Thordarson, *Chem. Soc. Rev.*, 2011, **40**, 1305–1323.
50 World Intellectual Property Organization International Bureau, WO 2010/056452 A2, 2009, 32.
51 A. Kotikian, C. Mcmahan, E. C. Davidson, J. M. Muhammad, R. D. Weeks, C. Daraio and J. A. Lewis, *Sci. Robot.*, 2019, **4**, eaax7044.